https://doi.org/10.1016/j.ymssp.2019.106410

Impaired Sound Radiation in Plates with Periodic Tunneled Acoustic Black Holes

Liling Tang [a, b] **and Li Cheng** [b*]

[a] *School of Marine Science and Technology, Northwestern Polytechnical University, Xi'an, China*

[b] *Department of Mechanical Engineering, The Hong Kong Polytechnic University, Hung Hom, Kowloon, Hong Kong, China*

[*]Corresponding author: li.cheng@polyu.edu.hk.

Phone: 852-2766 6769, fax: 852-2365 4703

Abstract

Acoustic Black Hole (ABH) effects offer remarkable possibilities to manipulate bending waves inside light weight structures. The effective frequency range of conventional ABH structures, however, is limited by the so-called characteristic/cut-on frequency, only above which can systematic ABH effects be systematically obtained, which seriously hampers practical applications. In this paper, plates with periodic tunneled double-leaf ABHs are studied to achieve reduced sound radiation in the low frequency range below the characteristic frequency. Upon showing the band structure of an infinite ABH lattice, the vibration and sound radiation of a finite plate with four ABH cells are investigated through FE analyses after experimental validations of the model. Results show that, apart from the expected ABH-induced benefit at high frequencies with damping treatment, it is also possible to draw acoustic benefit in the low frequency range, which is far below the characteristic frequency of the structure. It is shown that, within the ABH-induced locally resonant band gaps, the designed plates exhibit low sound radiation without additional damping treatment. Supersonic intensity and wavenumber analyses confirm that the observed phenomena are attributed to the impaired sound radiation efficiency

generated by the ABH-induced high energy localization inside the inactive sound radiation regions of the plate, alongside a structural wavenumber and vibration energy transport effect from supersonic to subsonic components when comparing to a uniform plate.

Keywords: *low frequency; acoustic reduction; Acoustic black hole; periodic plates.*

1. Introduction

Designing lightweight structures with low vibration and sound radiation has always been technically challenging and practically important. However, lightweight structures with traditional design are usually in conflict with the demand for low noise radiation and transmission. Recently, structural design based on the so-called Acoustic Black Hole (ABH) phenomenon shows new possibilities owing to its remarkable ability in tuning and manipulating bending waves inside structures such as beams and plates. Taking a one-dimensional beam as an example, the local phase velocity of the flexural waves reduces along the ABH beam with its thickness decreasing according to a power-law function, $h(x) = \varepsilon x^m \ (m \geq 2)$, thus achieving zero phase velocity and wave reflections at its end in an ideal scenario alongside an extremely high energy focalization [1-3]. Using simple and rather conventional ABH configurations, it has been shown that vibration energy and sound radiation can be impaired upon applying a small quantity of damping materials over the ABH area [4-9]. Existing numerical and experimental studies have also demonstrated the ability of ABH structures in multiple aspects pertinent to sound radiation control applications [7-9].

However, the effective frequency range, where ABH effects can be systematically achieved, is limited by the so-called characteristic or cut-on frequency where the incoming bending wavelength is comparable to or smaller than the characteristic dimension of the ABH cells [8, 10]. Consequently, it is infeasible to envisage low-frequency acoustic applications far below the characteristic frequency through conventional ABH design. The so-called conventional design infers to those

structures with simple ABH cells, namely tapers [11] and pits /indentations [7, 8], which are embedded into the structure, be it for beams or plates. In fact, existing research barely pays attentions to the low-frequency acoustic characteristics of ABH structures, arguably because of the well-accepted barrier due to the ABH cut-on.

Using a Rayleigh-Ritz model, our previous work [12] shows that, by capitalizing on the remarkable energy focalization and rich dynamics inside the ABH cells, locally resonant band gaps [13-15] can be achieved at relatively low frequencies in a beam with periodically arranged ABH cells [12]. For the analysis of such periodic lattice with ABHs, other potential methods may, in principle, also be used, such as impedance method [16], wave finite element [17, 18], boundary element [19], improved fast plane wave expansion [20] and extended plane wave expansion [21] approaches. Through introducing structural discontinuities inside the ABH elements [22], the energy focalization can also enhance the Bragg scattering effect [23, 24], thus extending the band gap to a broader higher frequency range. The combination of both local resonances and Bragg scattering generates wide band gaps within a large frequency range. These periodic ABH structures can be easily manufactured for effective vibration reduction using only a few cells. Such ABH design overcomes the limitations of conventional phononic crystals, in which Bragg band gaps usually require a large number of cells and a large lattice constant to reach low frequencies [25], or locally resonant band gaps are usually quite narrow [26]. Moreover, double-branched ABH design was shown to alleviate the inherent structural weakness of conventional ABH structures and maintain relatively high structural stiffness and strength [27], showing promise for practical applications.

Achieving the same objective in 2D planar structures turns out to be more challenging. Failing to obtain the absolute band gaps, a compromised solution was possible to generate directional band gaps for flexural waves with a proper ABH design. In fact, plates with periodically arranged tunneled double-leaf ABH was proposed [28]. The structure was shown to prohibit wave propagations along the

direction perpendicular to the ABH tunnel, and by the same token, confine vibration energy within an area close to the excitation. Despite the obvious benefit in terms of vibration insulation, how the generated energy concentration would affect the sound radiation remains unknown. This forms another main motivation of the present work, in conjunction with our interest in exploring possible low frequency ABH-specific phenomena.

Therefore, as a continuation of the previous work [28], sound radiations of plates with periodic tunneled double-leaf ABHs are investigated in this paper. Main focus is put on the low frequency range far below the characteristic frequency, typically within the two band gaps of the corresponding infinite ABH lattice. For the completeness of the paper, the band structure of an infinite ABH lattice is first shown. Then, the vibration and sound radiation properties of a finite plate with four ABH cells are investigated through FE analyses after experimental validations of the model. Supersonic intensity and wavenumber analyses are then carried out to shed lights on the underlying physics behind the observed impairment of the sound radiation efficiency of the plate and to reveal the physical changes in the ABH plate as compared with its uniform counterpart. Conclusions are then summarized in the least section of the paper.

2. Theoretical Background and Analysis Method

A plate with embedded double-leaf tunneled ABHs are investigated. The cross-sectional geometry of one unit-cell is shown in Fig. 1(a), which is to be periodically arranged along x-axis, forming either an infinite or finite plate. The tunnel is width-though in y-direction. The unit cell contains a double-branch ABH profile, each with a variable thickness $h(x)$ and connected by a strengthening stud. The wave propagating properties of the infinite periodic plate can be numerically investigated. The Floquet-Bloch 1D periodic boundary condition can be imposed at the edges of the unit-cell in x direction with a parametric sweep applied over the

reduced wave vector domain to obtain the dispersion curves of the structure.

When the plate is baffled in (x, y) plane and excited by a harmonic excitation force, the radiated acoustic pressure at an observation point (x, y, z) in an infinite free field can be obtained by [29]

$$p(x,y,z)=\frac{j\omega\rho_0}{2\pi}\int_{-b/2}^{b/2}\int_{-a/2}^{a/2}\frac{v(x',y',0)e^{-jkR}}{R}dx'dy', \tag{1}$$

where $\boldsymbol{v}$ is the normal velocity of the plate; $R=\sqrt{(x-x')^2+(y-y')^2+(z-0)^2}$; ω is the angular frequency of the plate, k and ρ_0 are the wavenumber and the air density, respectively. The time dependence $e^{j\omega t}$ is omitted for simplicity.

The radiated sound power is then obtained as

$$W=\frac{1}{2}\int_{-b/2}^{b/2}\int_{-a/2}^{a/2}\mathrm{Re}[p(x,y,0)v^*(x,y,0)]dxdy, \tag{2}$$

where the asterisk denotes the complex conjugate.

For analysis purposes, the sound radiation efficiency is defined as

$$\sigma=\frac{W}{\rho_0 cA\left\langle\overline{\boldsymbol{v}^2}\right\rangle}, \tag{3}$$

where c is the sound speed; A the surface area of the plate and $\left\langle\overline{\boldsymbol{v}^2}\right\rangle$ the averaged mean-square normal velocity of the plate, defined as $\left\langle\overline{\boldsymbol{v}^2}\right\rangle=\frac{1}{A}\int_{-b/2}^{b/2}\int_{-a/2}^{a/2}v(x,y,0)v^*(x,y,0)dxdy$.

Upon getting the above basic acoustic metrics, analyses will be performed through supersonic intensity and wavenumber analyses as detailed hereafter.

2.1 Supersonic intensity

Classical acoustic intensity, though very useful, does not allow easy

identification of the dominant vibration sources which are responsible for the far field sound radiation, especially in the subsonic frequency region below the critical frequency where subsonic structural wave components interact in a complex manner. Supersonic intensity is therefore introduced to filter out the subsonic waves and identify regions of a source that radiate effectively to the far field [30, 31].

The supersonic intensity is defined as

$$I^{(s)}(x,y,z)=\frac{1}{2}\mathrm{Re}\left\{p^{(s)}(x,y,z)v^{(s)}(x,y,z)^{*}\right\}, \tag{4}$$

where $\boldsymbol{p}^{(s)}$ and $\boldsymbol{v}^{(s)}$ denote the supersonic pressure and velocity respectively, which can be obtained in space domain directly through a two-dimensional convolution between the sound pressure (or velocity) and the radiation filter mask $h^{(s)}(x, y)$ [32] as follows:

$$p^{(s)}(x,y,z)=p(x,y,z)*h^{(s)}(x,y), \tag{5}$$

$$v^{(s)}(x,y,z)=v(x,y,z)*h^{(s)}(x,y), \tag{6}$$

in which $h^{(s)}(x, y)$ is used to filter the subsonic wave, expressed as $h^{(s)}(x,y)=\frac{k}{2\pi\sqrt{x^2+y^2}}J_1(k\sqrt{x^2+y^2})$ with J_1 being the Bessel function of the first kind.

2.2 Wavenumber transforms

Wavenumber spectra decompose the vibration field into different wavenumber components, which indicate both the direction and the strength of the waves [33, 34]. Wavenumber components show the distribution of vibration energy in supersonic and subsonic waves respectively through the amplitude of the wavenumber spectrum. These features are exploited here to understand the sound radiation mechanisms of the ABH structures.

For a given frequency f, the velocity field $v(x,y,f)$ in spatial domain is transformed into the wavenumber domain through a two dimensional Fourier transform as

$$V(k_x,k_y,f)=\int_{-b/2}^{b/2}\int_{-a/2}^{a/2}v(x,y,f)e^{-jk_x x}e^{-jk_y y}dxdy, \tag{7}$$

where k_x and k_y are the wavenumbers in the x and y directions, respectively.

3. Finite element model and experimental validations

3.1 Finite element analyses

Referring to Fig. 1(a), the thickness of each half ABH branch takes the form of $h(x)=48.4375(x-0.015)^3+0.0005$ with a length of l_{ABH}=0.04m and a residual thickness h_0=0.0005m. The length of the strengthening stud is $l_s=0.03$ m. The unit cell has a length a=0.16m and a height h=0.007m. The section is extended along y direction with a width b=0.3m to form the three-dimensional model of the unit-cell. The wave propagating characteristics of the infinite periodic plate are firstly investigated using Solid Mechanics Module of COMSOL Multiphysics. The 1D Floquet-Bloch periodic boundary condition is imposed at the edges of the unit cell in x direction and a parametric sweep is applied over the reduced wave vector $\boldsymbol{ka/\pi}$. The meshing detail of the unit-cell is shown in Fig.1 (b) with a total of 5760 hexahedrons elements to guaranty a minimum of 6 elements per wavelength at the highest frequency of interest, namely 5000 Hz, while ensuring a truthful geometrical description of the structural profile at the same time. The plate is made of steel with a mass density ρ of 7850 kg/m^3, Young's modulus E of 200 Gpa, Poisson's ratio σ of 0.28 and a material damping loss factor η of 0.001. Using the thickness of the uniform part of the plate, the critical frequency of the plate, above which flexural waves are supersonic and efficient in sound radiation, is calculated by $f_c=\frac{c^2}{2\pi}\sqrt{\frac{12\rho(1-\upsilon^2)}{Eh^2}}$

[35], giving 1760 Hz in the present case. The cut-on/characteristic frequency of the plate [8, 10] is estimated as 4170 Hz, obtained from $f_{\text{Char}} = \frac{\pi}{l_{\text{ABH}}^2}\sqrt{\frac{Eh^2}{3\rho(1-\upsilon^2)}}$. Above the cut-on/characteristic frequency, the incoming flexural wavelength is comparable or smaller than the characteristic dimension of the ABH cells, thus entailing systematic ABH effects.

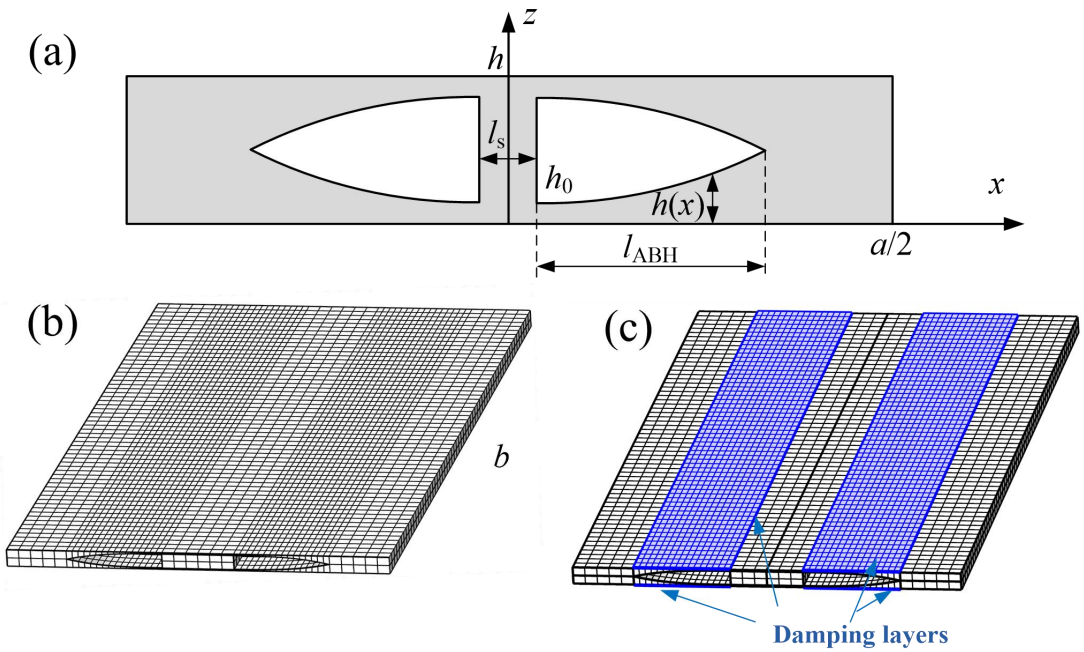

Fig. 1 (a) Cross section of one unit-cell; (b) mesh details of the unit cell; (c) unit cell with damping layers.

3.2 Band structures of an infinite ABH lattice

For the completeness of the paper, the band structure of the ABH plate is briefly recalled. Details can be found in [28]. It is relevant to note that, since the main target of the proposed plate design is to achieve effective insulation in vibration energy propagation, and then hopefully reduced sound radiation, only propagating modes are considered here. The evanescent modes can be calculated by the extended plane wave expansion [17, 21] if necessary. Fig. 2 depicts the dispersion curves, which show multiple rather flat curves, showing locally resonant characteristics with approximate

zero group velocity. This is attributed to the ABH-induced energy focalization effect, which can be exemplified by two representative modes L_1 and L_2. For mode L_1, ABH branches act as springs and behave like local resonators together with the strengthening stud. For mode L_2 at relatively high frequency, the ABH parts still roughly act as local resonators with high energy focalization. Meanwhile, a large impedance mismatch between the strengthening stud and the ABH branches generates the Bragg scattering effect. Although these flat dispersion curves are intersected by two curves corresponding to the S0 and SH0 modes, respectively, broad band gaps can still be achieved (as denoted by grey shadowed areas in Fig. 2) if only flexural waves are to be considered. More detailed analyses, as well as the formation mechanisms of the gaps, can be found in our previous work [28]. Periodic ABH plates with such broad band gaps show high wave filtering effect and can enable effective vibration isolation by using only a few cells [28]. However, as mentioned previously, the effect of high energy focalization within band gaps on the sound radiation of the periodic plate remains unknown.

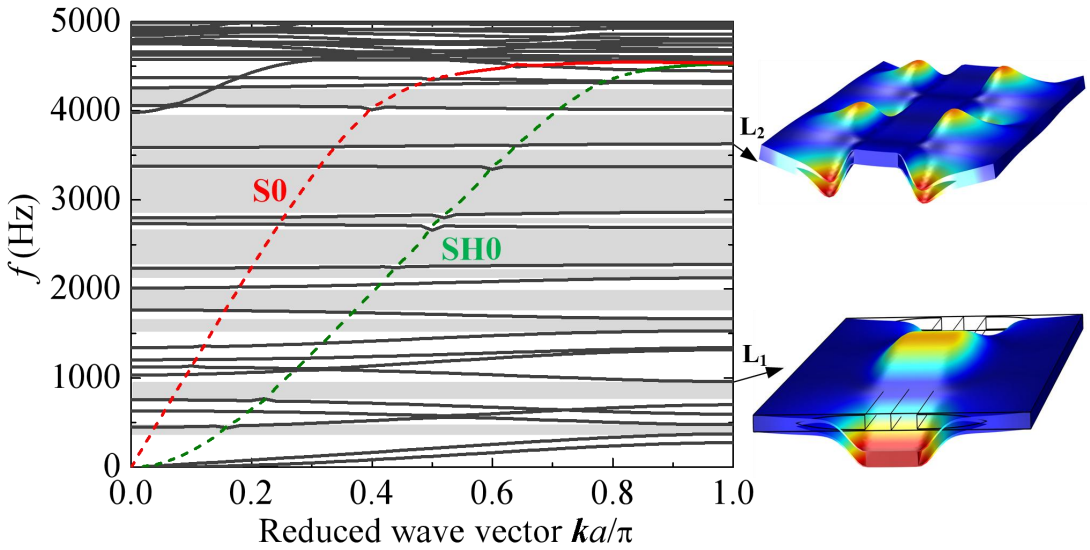

Fig. 2 Band structures of the infinite periodic plates with grey shadowed areas denoting band gaps only for flexural waves.

3.3 Sound radiation modelling

To explore the acoustic characteristics of such periodic plate structures, a periodic plate with four ABH cells is analyzed under a unit harmonic force excitation. The force is located at a point, offset the center of the plate along y direction by 0.02 m, as shown in Fig. 3(a). With the consideration of the coupling between the plate and the surrounding air, the plate is modeled in the Acoustic-Solid Interaction Module of COMSOL, as shown in Fig. 3(b). The plate is treated as baffled, in contact with air on one side. The acoustic field is modeled as a semi-sphere with a radius which is large enough to comply with the far-field approximation. The semi-sphere air domain is meshed using free tetrahedral elements whilst the mesh of each cell of the plate being kept the same as in Fig. 1(b). The meshing is verified to be sufficiently dense to resolve the vibration and acoustic field and fully capture the ABH features at the highest frequency considered in this paper, 5 kHz. Nominal acoustic parameters are used: c=343 m/s and $\rho_0 = 1.21$ kg/m^3. Upon obtaining the normal velocity of each grid node of the plate $\boldsymbol{v}$, the radiated acoustic pressure can be obtained by using the discrete forms of Eq. (1), *i.e.* $p(x,y,z) = \frac{j\omega\rho_0}{2\pi}\sum_{\Delta S}\frac{ve^{-jkR}}{R}\Delta S$, with ΔS being the area of each element. Similarly, the radiated sound power, sound radiation efficiency and supersonic intensity can also be calculated using the discrete forms of Eqs. (2) to (6) through summations instead of integrals.

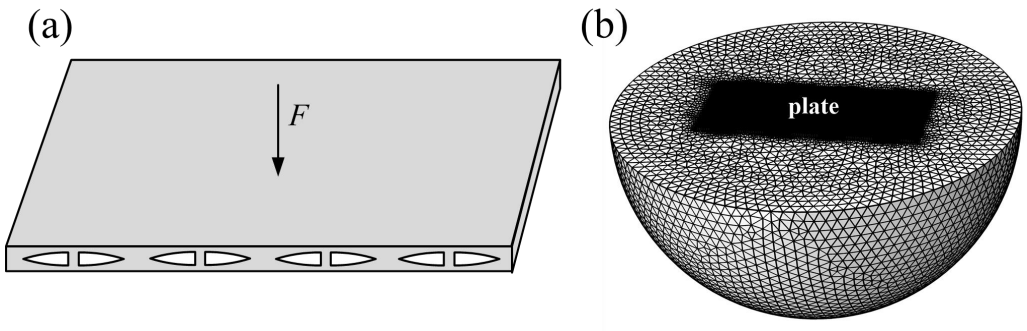

Fig.3 (a) Sketch of a periodic plate with four ABH cells under a unit harmonic force F; (b) mesh overview of the model.

3.4 Experimental validations of the FE models

Experiments were conducted to validate the finite element models. Both the periodic ABH plate with four ABH cells and the corresponding uniform plate were tested in an anechoic chamber having a dimension of 6 m×6 m× 3 m and a cut-off frequency of 80 Hz. The geometrical and material parameters of the panels are the same as those used in numerical simulations. As shown in Fig. 4 (a), the tested plate was hanged by two thin strings on the center of a large wooden baffle with a dimension 2.44×2.44×0.02m to achieve free boundary conditions. This realization is easier to achieve than the clamped boundaries due to the high stiffness of the tested plates. However, precautions were taken to seal the tiny air gaps between the plate and the baffle to avoid possible acoustic short-circuiting effects, where sound pressures from the front and back of the plate may interact with each other, thus minimizing the pressure differences. The plate was excited by an electromagnetic shaker with a force transducer on the back side, where a tiny accelerometer was also attached for vibration measurement. The locations of the applied force and the accelerometer are sketched in Fig. 4 (a). The sound pressure level $L_p = 20\lg\frac{p}{p_{\text{ref}}}$ was obtained by 20 microphones with $\mathrm{p_{ref}} = 20\mu\mathrm{Pa}$. Locations of the microphones were chosen according to ISO 3744 [36] over a hemisphere with a radius r of 1.22m. The average sound pressure level and the radiated sound power level are then obtained. A experimental sketch with specifications of the measurement instruments is also given in Fig. 4 (b).

The numerically calculated acceleration and sound power level are compared with the experimental measurements in Fig. 5. It can be seen that for both the uniform and the ABH plates, the two sets of results agree reasonably well with each other, in terms of both peak locations and amplitude levels, especially in the low-frequency range, which is our main scope of interest. Some additional peaks, especially in the frequency band from 1200 Hz to 2000 Hz for the uniform plate, are caused by the torsional waves induced by the slightly deviation of excitation force from the vertical plane. Therefore, the numerical model is deemed reliable and accurate enough, as far

as the low frequency range is concerned.

(a)

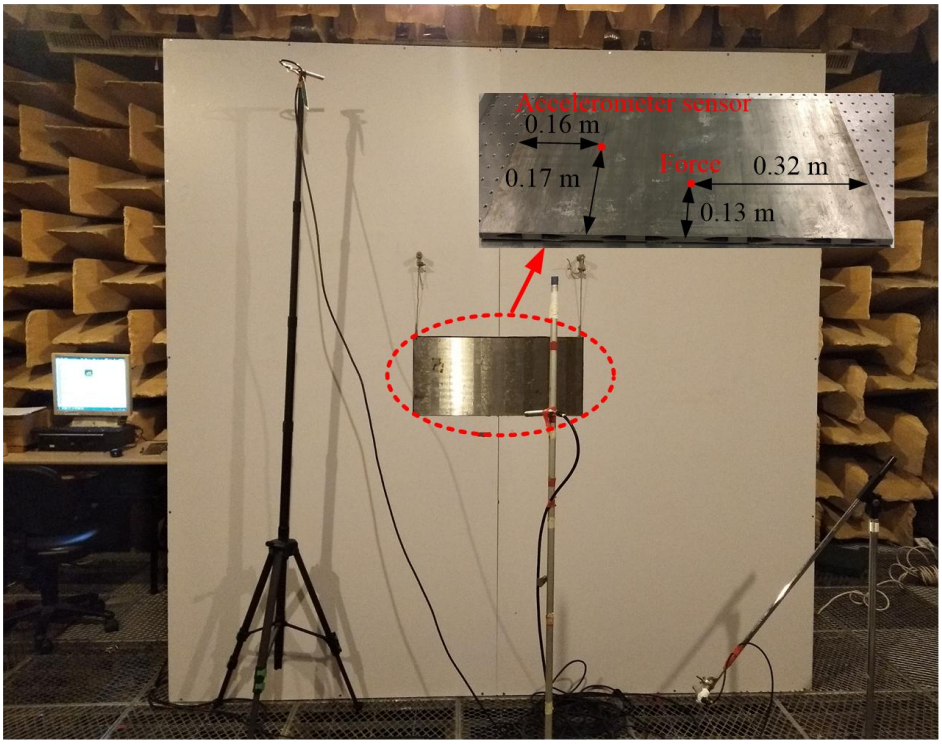

(b)

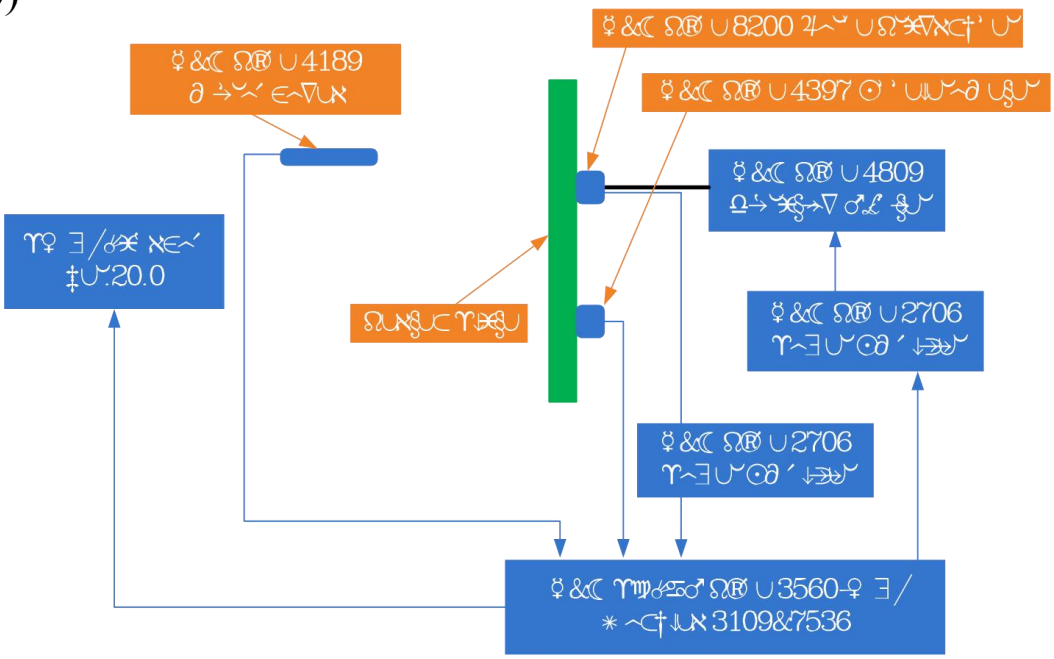

Fig. 4 Experimental (a) setup and (b) sketch

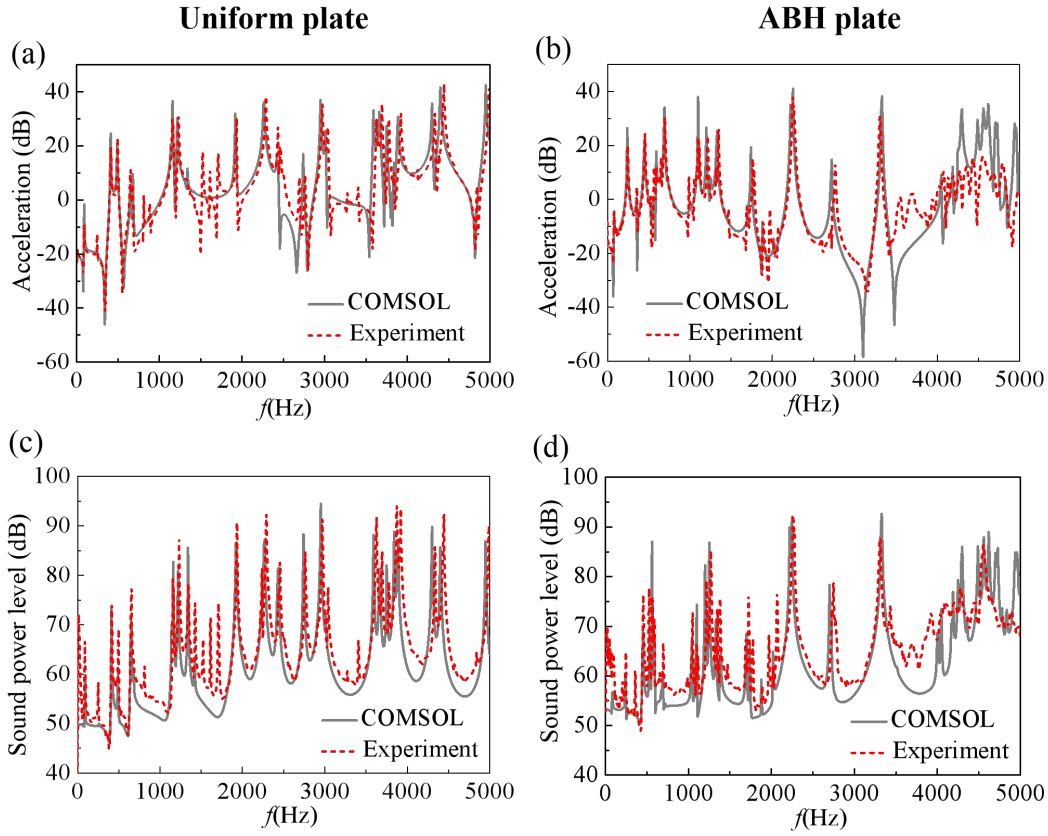

Fig. 5 Comparisons of the acceleration and sound power level from COMSOL results against experimental measurements.

4. Results and discussions

The above established FEM model is used for analyses. Considering the wider application, clamped boundary conditions are applied to the plates in the following analyses. To quantify the low-frequency acoustic characteristic below the characteristic frequency, a normalized dimensionless frequency is defined as $f_{\mathrm{Norm}} = f / f_{\mathrm{Char}}$, where f_{Char} is the characteristic frequency, which is 4170 Hz in the present case. Therefore, the two band gaps obtained before are all well below the characteristic frequency with a f_{Norm} much smaller than 1. Therefore, the corresponding frequency bands are referred to as the low frequency thereafter.

The mean quadratic velocity and the sound power level of the ABH plate are first compared with the referenced uniform plate in Figs. 6 (a) and (c), respectively. Since

no damping layers are applied to the plates, advantages of the ABH plates over its uniform counterpart cannot be obviously seen in terms of vibration reduction, nor the overall sound reduction, as shown in Figs. 6(a) and (c). This is definitely due to the weakened stiffness of the ABH plates as well as the absence of the damping treatment. However, a close examination of the two band gap areas at low frequencies marked in grey color shows that, although the mean quadratic velocity of the ABH panel is rather high (even higher than that of the uniform panel), the corresponding sound radiation by the ABH panel is lower even without using additional damping layers.

The above observed phenomena are re-examined when damping layers are applied over the ABH portion of the ABH panel and the corresponding area in the uniform panel, respectively, as show in Fig. 1 (c). In both cases, the applied damping layers have a thickness of 0.001 m, a mass density of 950 kg/m^3, Young's modulus of 5 Gpa, Poisson's ratio of 0.3 and a damping loss factor of 0.1. As shown in Figs. 6 (b) and (d), a systematical reduction, up to 20 dB, in both vibration level and the radiated sound power, can be observed above the characteristic frequency as compared to the uniform plate, due to the fully achieved ABH effect. In that region, systematic ABH effect dominates the system response due to the enhanced broadband energy absorption through damping layers. Interesting enough, inside the two low frequency band gaps, the deployment of the damping layers would not necessarily help further reduce the sound radiation as indicated in Fig. 6(d), although the sound power level still remains systematically lower than the uniform plate. The plausible reason is that, as demonstrated earlier, these band gaps are due to locally resonant behavior, thus requiring strong dynamics of the local oscillators. This can be better achieved without the damping layer.

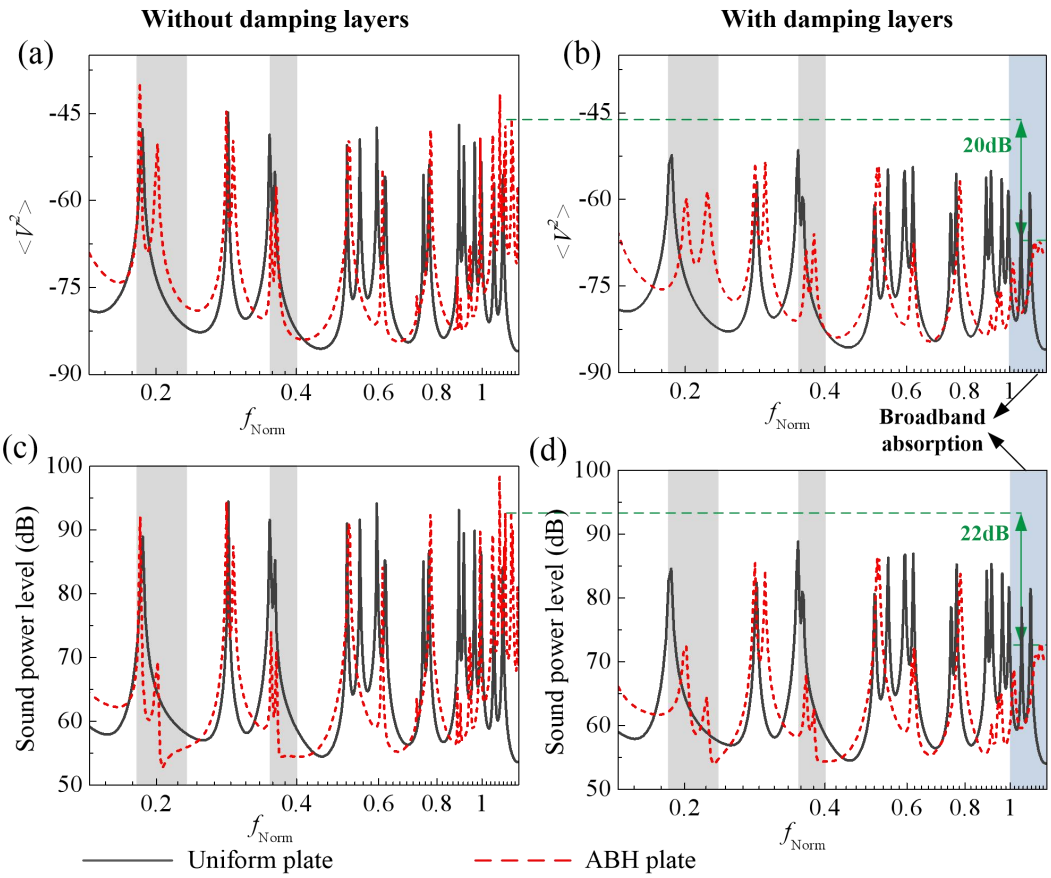

Fig.6 Mean quadratic velocity and sound power level comparisons between different plates with/without damping layers (grey areas denote the two low frequency band gaps in the infinite periodic ABH plate).

The observed reduction in the sound radiation within the band gaps at quite low frequencies even without damping layers points at the possibility for low-frequency noise control using ABH structures and deserves further exploration. To better understand the intrinsic changes inside the plate as a result of the inclusion of the ABH cells, the corresponding radiation efficiency is calculated with results shown in Fig. 7 for both uniform and ABH plates, with/without damping layers. As can be seen, the radiation efficiency of the ABH panel is systematically lower than that of the uniform panel above the critical frequency (1760 Hz in the present case), which is due to ABH-induced slowing-down of the wave speed. In the process, the acoustical faster structural waves, also referred to as supersonic structural waves, are partly converted to subsonic inside a certain portion of the ABH area [8, 9], making the structure less

radiation efficient. However, this reduction in the radiation efficiency is not obvious compared with existing ABH structures, which is caused by the scattering effect of the strengthening studs. Below the critical frequency, two obvious dips appear for the ABH panel at very low frequencies with a maximum reduction reaching roughly 22 dB. Particularly, these two reduction ranges roughly coincide with the two band gaps at low frequencies (also marked by grey areas), consistent with the observations on the sound radiation. Therefore, despite the strong energy focalization, the overall sound radiation efficiency of the ABH panel is greatly reduced, in regions which are far below the characteristic frequency of the panel. With added damping layers, Fig. 7 shows negligible effect on the uniform panel, but a slight increase in the radiation efficiency of the ABH plate after the critical frequency due to the increased structural stiffness, consistent with the previous observation made in Ref. [9]. The deployment of the damping layers, however, shifts the weak radiation frequency range before the critical frequency to higher frequencies, but still within the band gaps. The observed reduction in the sound radiation efficiency of the ABH plate explains the observed sound radiation in the low frequency range despite the fact that the vibration level may not be systematically reduced or even increased as observed in Fig. 6(a).

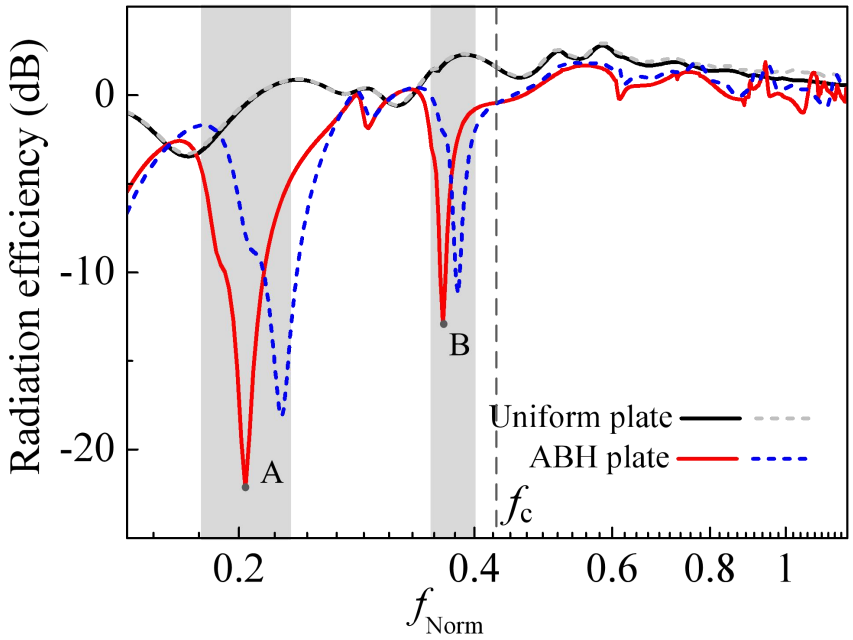

Fig.7 Radiation efficiency comparison between different plates: solid lines denote

cases without damping layers; dashed lines denote cases with damping layers; grey dark areas denote band gaps in infinite periodic ABH plate without damping layers.

The following analyses mainly focus on the cases without damping layers to reveal the underlying physical mechanism within the two band gaps. The velocity response, supersonic intensity and the wavenumber spectra are computed and analyzed at selected representative frequencies inside the two dip region of the sound radiation efficiency curves (marked as A and B in Fig. 7, respectively). Results on the uniform panel are also presented as a comparison basis, although the two plates are different vibration systems even at the same driving frequency.

The velocity response and the corresponding supersonic intensity of the first radiation efficiency dip at frequency A are illustrated in Fig. 8. For the uniform plate, the supersonic intensity map and the velocity distribution are highly consistent, showing that far field sound radiation is mainly due to the energetic part of the plate. For the ABH plate, however, although strong vibrations rather reside in the central area of the plate, sound is mainly emitted from the two edges of the ABH plate where the vibration level is rather weak. The observed vibration energy concentration is due to the band gap effect of the plate which confines the vibration energy to the central area where the plate is excited. Moving away from the center, flexural waves are prohibited when passing through the nearby ABH element. Therefore, at this frequency, the radiation of the ABH plate is mainly from the two edges where vibration energy is low.

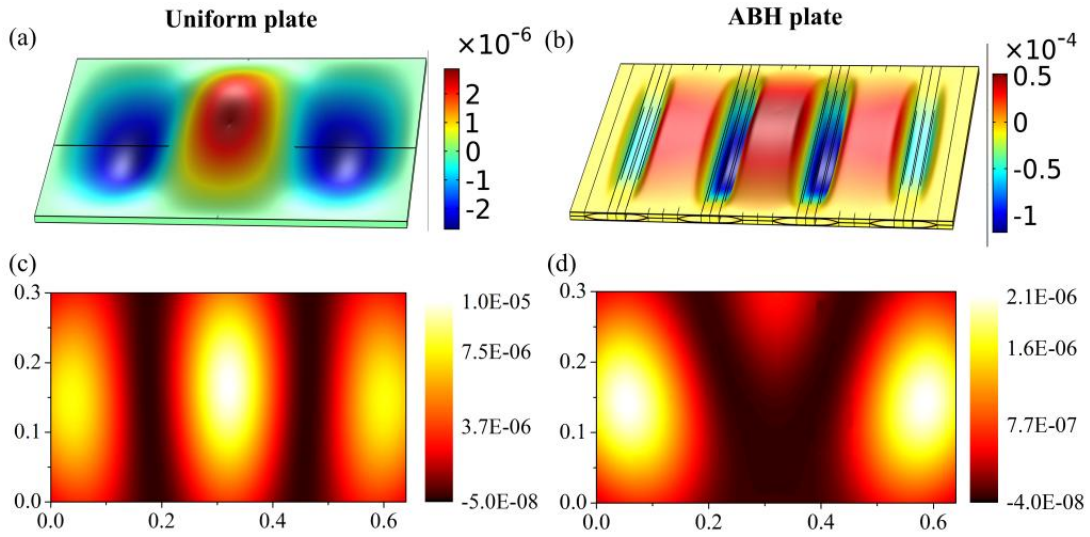

Fig. 8 Velocity response: (a), (b) and supersonic intensity: (c), (d) of the uniform plate and the ABH plate at frequency A as marked in Fig. 7.

To further reveal the physical changes in the plate due to the inclusion of the ABH cells, corresponding wavenumber spectra of the square of the wavenumber transform of the velocity are examined, the amplitude of which represents the energy distribution in the wavenumber domain. A so-called radiation circle is also included at the given frequency *f*, along which the acoustic wavenumber equals to the structural wavenumber, namely $k_x^2+k_y^2=k_c^2=\left(\frac{2\pi f}{c}\right)^2$, where k_c is the acoustic wavenumber. Within this circle, structural wave components are supersonic with efficient sound radiation to the far field. On the contrary, energy components outside the radiation circle are subsonic with minimum sound contribution to the far field.

The wavenumber spectra of the uniform and ABH plates at the same frequency marked as A are compared in Fig. 9 (a) and (b). As can be seen, the uniform plate possesses high vibration energy level inside and around the radiation circle. Therefore, a significant part of the vibration components is supersonic, thus radiating effectively to the far field and resulting in a relatively high radiation efficiency as shown in Fig. 7. However, for the ABH plate, the overall velocity level is higher than the uniform plate because of the reduced thickness and consequently weaker stiffness. However,

vibration energy is distributed across the radiation circle and tends to spread to higher wavenumber domain, especially in *x* direction. By so doing, the major portion of the vibration energy is subsonic with little contribution to the far filed sound radiation. In a sense, the arrangement of the periodic ABH elements in *x* direction and the resultant ABH effect generate a structural wavenumber and vibration energy transport effect from supersonic to subsonic components when comparing to a uniform plate.

Cases with damping layers are also analyzed with results shown in Fig. 9 (c) and (d) to check the effect of the damping layers. With damping layers, the overall vibration level and energy distribution of the uniform plate remain almost the same, where major vibration components are supersonic and radiate effectively. For the damped ABH plate, the overall vibration level is reduced because of the obvious increased energy dissipation. Meanwhile, the vibration energy still spread to higher wavenumber domain with a major portion being subsonic. Interestingly, the supersonic energy components within the radiation circle are slightly higher than their counterparts without damping layers, demonstrating the stronger acoustic radiation characteristics. This is because damping layers increase the thickness of the ABH part and impair the energy transport from supersonic to subsonic to some extent, which is consistent with the increased sound radiation and radiation efficiency at this frequency as observation from Figs. 6 and 7.

Similar analyses are carried out for the second dip frequency on the sound radiation efficiency curves (marked as B in Fig. 7), with results shown in Figs. 10 and 11, respectively. The results show very similar phenomena as those observed for the first one. As shown in Fig.10, the band gap effect of the ABH plate first alters the vibration energy distribution over the plate, from rather uniform distribution over the plate to a rather concentrated one, in the central ABH areas close to the force excitation area. Waves, originating from the excitation position, quickly get attenuated

when passing through the first ABH element because of the locally resonant effect. Supersonic intensity results also show that the effective radiation region is the uniform part between the two adjacent ABH channels, where the vibration level is rather low. Furthermore, the wavenumber spectra in Fig. 11 (a) and (b) show that, although the overall vibration energy level in both plates is comparable, supersonic components within the radiation circle are quite different. The reduced supersonic energy components of the ABH plate explain the observed impairment of its sound radiation and radiation efficiency. Again, with damping layers applied in Fig. (c) and (d), the supersonic energy components of the ABH plate are still lower than these of the uniform plate, but higher than the ABH plate without damping layers, demonstrating that damping layers offer no further improvement on sound radiation within these two band gaps.

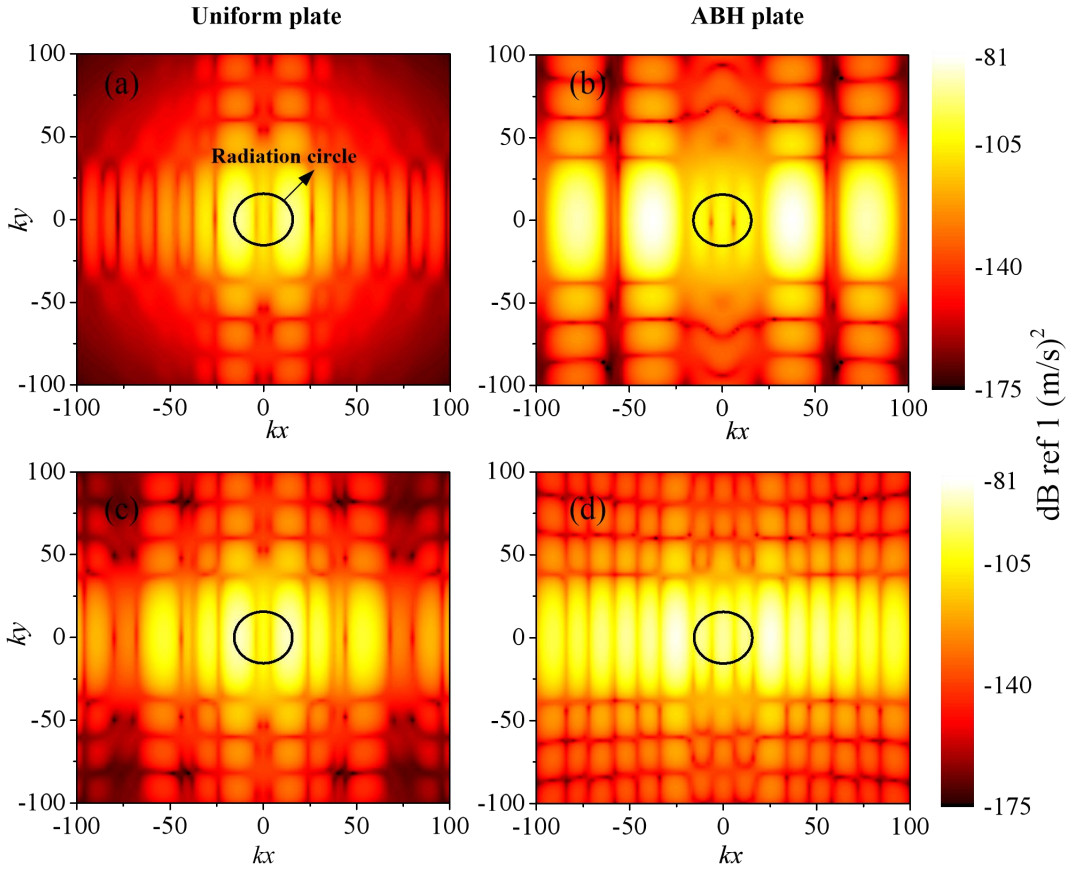

Fig. 9 Wavenumber spectra of uniform plate and ABH plate without: (a), (b) and with: (c), (d) damping layers at frequency A.

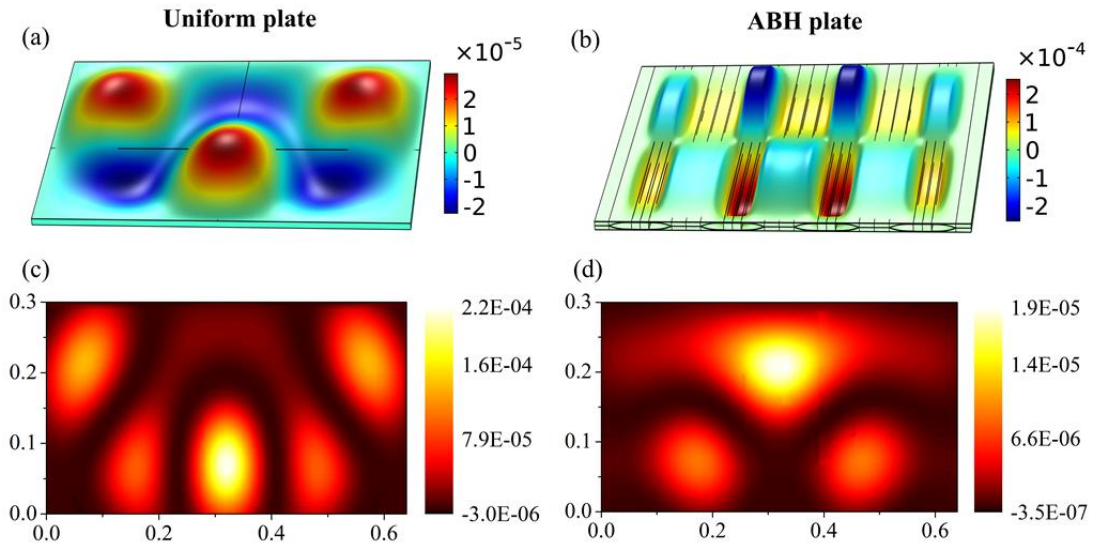

Fig. 10 Velocity response: (a), (b) and supersonic intensity: (c), (d) of the uniform plate and the ABH plate at frequency B as marked in Fig. 7.

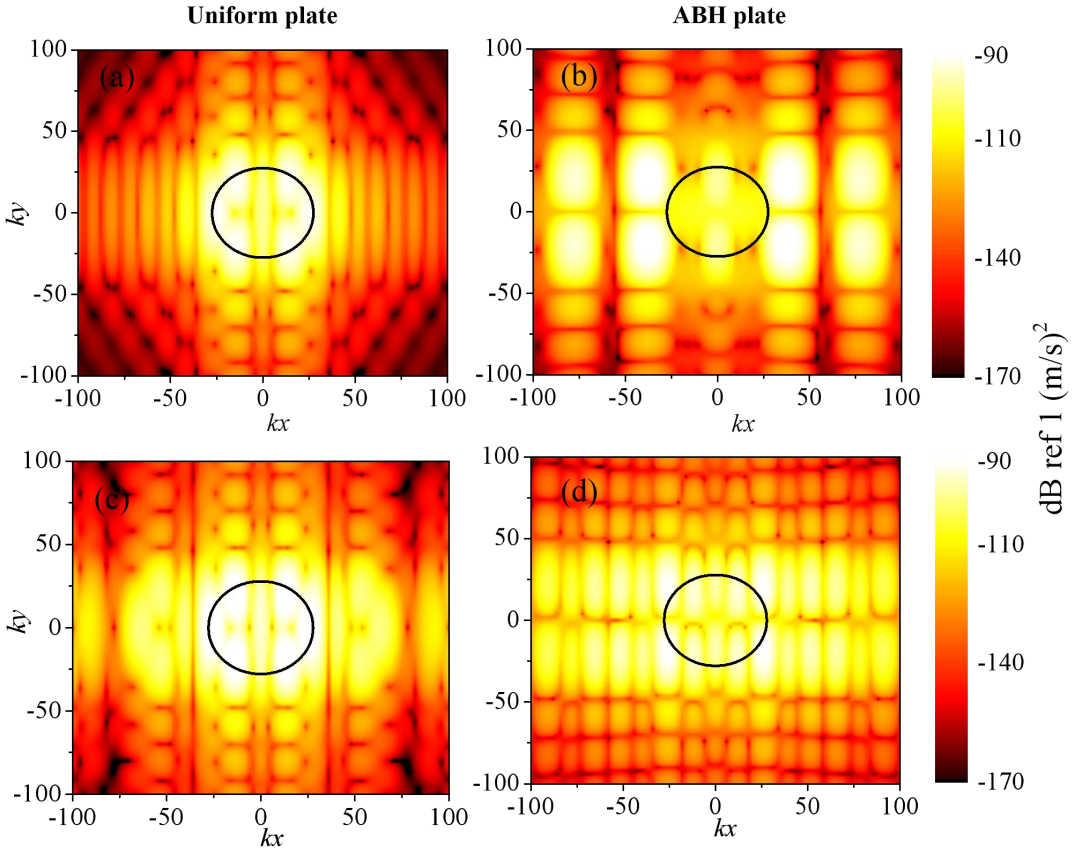

Fig. 11 Wavenumber spectra of uniform plate and ABH plate without: (a), (b) and with: (c), (d) damping layers at frequency B.

As a final result, variations of the sound radiation efficiency of the periodic ABH plate with different number of cells are shown in Fig. 12. As can be seen, the number of cells would not alter the locations of the two dips, but only change the reduction level of the sound radiation efficiency. More cells would in principle improve the sound radiation properties of the plate, for example from 2 to 6. However, further increasing the number of cells may not bring up significant improvement, since as reported before, the proposed structure allows the formation of quasi-band gap with a very small number of cells, which is again attributed to the specific features of the ABH. Furthermore, the effective frequency range of the reduction of radiation efficiency and sound radiation corresponds to the band gaps, mainly caused by the local resonances of the ABH part. Unlike conventional tuner resonators targeting at single resonant frequency, each ABH cell acts as a continuous local resonator with multiple degrees of freedoms, thus entailing multiple broad band gaps. Therefore, particular frequency band can be targeted by tuning the ABH parameters and the length of strengthening stud. Parametric analyses on the band gaps can be found in our previous work [28].

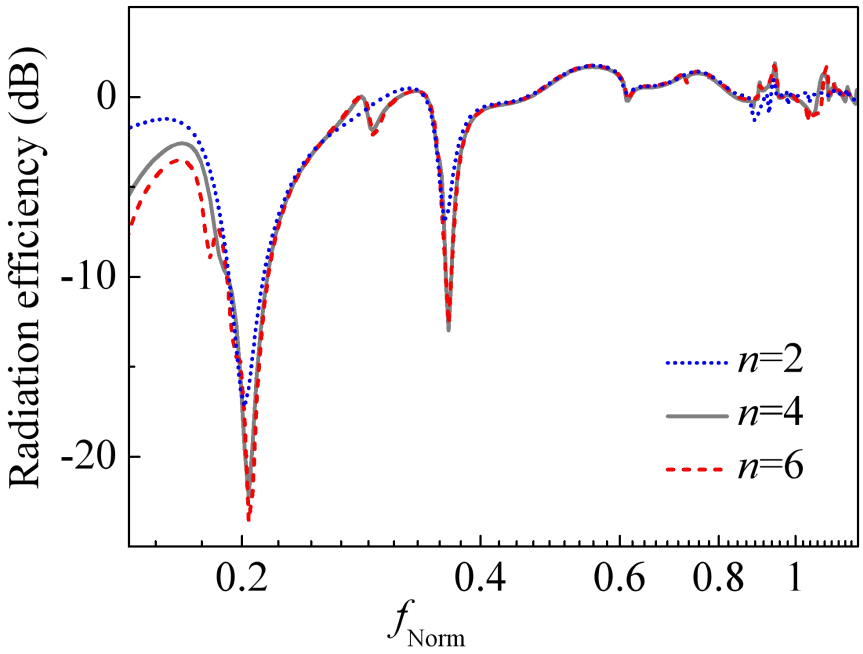

Fig. 12 Radiation efficiency of periodic ABH plates with different number of ABH cells.

5. Conclusions

In an attempt to reduce the lower limit of ABH-based structural design, this paper investigates the sound radiation properties of a plate with periodically arranged double-leaf ABH channels. Main focus is put on the low frequency range, typically below the characteristic/cut-on frequency of the plate. Upon showing the band structure of the infinite ABH lattice, a finite plate with four ABH cells is investigated through FE analyses after experimental validations of the model. Main conclusions are drawn as follows.

1) Apart from the expected ABH-induced benefit at high frequencies with damping treatment, beneficial acoustic effect can also be materialized in the low frequency range, which is typically far below the characteristic frequency of the structure. Compared with its uniform counterpart, the channeled double-leaf ABH plate features a broadband reduction in its sound radiation efficiency without additional damping treatment. The phenomenon is particularly striking within the low frequency band gaps of the corresponding infinite periodic panel in which the impairment of the sound radiation efficiency is drastic.

2) Supersonic intensity and wavenumber analyses allow identifying the dominant sound radiation regions over the ABH plate and describing the physical changes inside the plate due to the inclusion of the ABH cells.

3) The basic mechanisms behind the significantly impaired low sound radiation efficiency of the ABH plate at low frequencies are twofold: one being the energy focalization within the excited area of the plate as a result of the previously discovered directional band gap behavior of the proposed structure; and the other one being the conversion of the supersonic vibration components to subsonic ones due to the reduction in the phase velocity of the waves. Both effects are ABH-specific, which are particularly evident inside the locally resonant band gaps obtained from an infinite ABH lattice. With both effects

combined together, regions containing high vibration energy but low sound radiation efficiency are created in the ABH plate, thus warranting a reduced sound radiation into the far field.

As a final remark, the designed tunneled ABH plates show attractive features for potential industrial applications. On one hand, this kind of light-weight ABH plates can achieve sound reductions at low frequencies even without additional damping treatment. On the other hand, it maintains structural surface integrity and offers improved structural stiffness as compared with conventional single-layer ABH plates. This enables the use of such structures in industrial applications for sound reduction purposes or as structural components with reasonable load-bearing capacity. The down-side of the design is the added complexities to structural geometry and its manufacturing. Meanwhile, due to the one-directional ABH tunnel, the vibration isolation and sound reduction is also directionally effective. The investigation of more complex and generic 2D periodic ABH plate would be our future work.

Acknowledgements

The authors would like to thank the financial support from the Research Grant Council of the Hong Kong SAR (PolyU 152017/17E), National Science Foundation of China (No. 11532006; No. 11902260), and Fundamental Research Funds for the Central Universities (No. 3102019HHZY03001).

References

[1] M.A. Mironov, Propagation of a flexural wave in a plate whose thickness decreases smoothly to zero in a finite interval, *Soviet Physics: Acoustics* 34 (3) (1988) 318-319.

[2] V.V. Krylov, and F. J. B. S. Tilman, Acoustic 'black holes' for flexural waves as effective vibration dampers, *Journal of Sound and Vibration* 274 (2004) 605-619.

[3] H. Ji, J. Luo, J. Qiu, and L. Cheng, Investigations on flexural wave propagation and attenuation in a modified one-dimensional acoustic black hole using a laser excitation technique, *Mechanical Systems and Signal Processing* 104 (2018) 19-35.

[4] J. Deng, L. Zheng, P. Zeng, Y. Zuo, and O. Guasch, Passive constrained viscoelastic layers to improve the efficiency of truncated acoustic black holes in beams, *Mechanical Systems and Signal Processing* 118 (2019) 461-476.

[5] D.J. O'Boy, E.P. Bowyer, and V.V. Krylov, Point mobility of a cylindrical plate incorporating a tapered hole of power-law profile, *The Journal of the Acoustical Society of America* 129(6) (2011) 3475-3482.

[6] L.L. Tang, L. Cheng, H.L. Ji, and J.H. Qiu, Characterization of acoustic black hole effect using a one-dimensional fully-coupled and wavelet-decomposed semi-analytical model, *Journal of Sound and Vibration* 374 (2016) 172-184.

[7] E.P. Bowyer and V.V. Krylov, Experimental study of sound radiation by plates containing circular indentations of power-law profile, *Applied Acoustics* 88 (2015) 30-37.

[8] S.C. Conlon, J.B. Fahnline, and F. Semperlotti, Numerical analysis of the vibroacoustic properties of plates with embedded grids of acoustic black holes, *The Journal of the Acoustical Society of America* 137(1) (2015) 447-457.

[9] L. Ma, and L. Cheng, sound radiation and transonic boundaries of a plate with an acoustic black hole, *The Journal of the Acoustical Society of America* 145 (2019) 164-172.

[10] L.L. Tang, and L. Cheng, Enhanced Acoustic Black Hole effect in beams with a modified thickness profile and extended platform, *Journal of Sound and Vibration* 391 (2011) 116-126.

[11] X. Li, and Q. Ding, Sound radiation of a beam with a wedge-shaped edge

embedding acoustic black hole feature, *Journal of Sound and Vibration* 439 (2019) 289-299.

[12] L.L. Tang and L. Cheng, Broadband local resonant bandgaps in periodic structures with embedded acoustic black holes, *Journal of Applied Physics* 121(2017) 194901.

[13] Z. Liu, X. Zhang, Y. Mao, Y. Zhu, Z. Yang, C. Chan, and P. Sheng, Locally resonant sonic materials, *Science* 289 (5485) (2000)1734-1736.

[14] E.J.P. Miranda Jr., E.D. Nobrega, A.H.R. Ferreira, and J.M.C. Dos Santos, Flexural wave band gaps in a multi-resonator elastic metamaterial plate using Kirchhoff-Love theory, *Mechanical Systems and Signal Processing* 116 (2019) 480-504.

[15] L. Raghavan and A.S. Phani, Local resonance bandgaps in periodic media: theory and experiment, *The Journal of the Acoustical Society of America* 134 (2013) 1950-1959.

[16] V.B. Georgiev, J. Cuenca, F. Gautier, L. Simon, V.V. Krylov, Damping of structural vibrations in beams and elliptical plates using the acoustic black hole effect, *Journal of Sound and Vibration* 330 (2011) 2497-2508.

[17] E.J.P. Miranda Jr., J.M.C. Dos Santos, Flexural wave band gaps in phononic crystal Euler-Bernoulli beams using wave finite element and plane wave expansion methods, *Materials Research* 20 (2017) 729-742.

[18] E.D. Nobrega, F. Gautier,; A. Pelat, J.M.C. Dos Santos, Vibration band gaps for elastic metamaterial rods using wave finite element method, *Mechanical Systems and Signal Processing* 79 (2016) 192-202.

[19] F.L. Li, Y.S. Wang, C. Zhang, G.L. Yu, Boundary element method for band gap calculations of two-dimensional solid phononic crystals, *Engineering Analysis with Boundary Elements* 37 (2013) 225-235.

[20] L. Xie, B. Xia, J. Liu, G. Huang, and J. Lei, An improved fast plane wave expansion method for topology optimization of phononic crystals. *International*

Journal of Mechanical Sciences 120 (2017) 171-181.

[21] E.J.P. Miranda Jr., and J.M.C. Dos Santos, Evanescent Bloch waves and complex band structure in magnetoelectroelastic phononic crystals, *Mechanical Systems and Signal Processing* 112 (2018) 280-304.

[22] L.L. Tang, and L. Cheng, Ultrawide band gaps in phononic beams with double-leaf acoustic black hole indentations, *The Journal of the Acoustical Society of America* 142 (2017) 2802-2807.

[23] A. Martin, M. Kadic, R. Schittny, T. Bückmann, and M. Wegener, Phonon band structures of three-dimensional pentamode metamaterials, *Physical Review B* 86 (2012)155116.

[24] J. H. Ma, Z. L. Hou, and B. M. Assouar, Opening a large full phononic band gap in thin elastic plate with resonant units, *Journal of Applied Physics* 115 (2014) 093508.

[25] L. Brillouin, Wave Propagation in Periodic Structures, 1946 New York: McGraw-Hill.

[26] L. Raghavan, A. Srikantha Phani, Local resonance bandgaps in periodic media: Theory and experiment, *The Journal of the Acoustical Society of America* 134(3) (2013) 1950-1959.

[27] T. Zhou, L.L. Tang, H.L. Ji, J.H. Qiu, and L. Cheng, Dynamic and static properties of double-layered compound acoustic black hole structure, *International Journal of Applied Mechanics* 9 (2017) 1750074.

[28] L.L. Tang and L. Cheng, Periodic plates with tunneled Acoustic-Black-Holes for directional band gap generation, *Mechanical Systems and Signal Processing* 133 (2019) 106257.

[29] F. Fahy and P. Gardonio, Sound and structural vibration: radiation, transmission and response, *Elsevier/Academic*, Oxford, 2007.

[30] E.G. Williams, Supersonic acoustic intensity, *The Journal of the Acoustical Society of America* 97(1) (1995) 121-127.

[31] E.G. Williams, Supersonic acoustic intensity on planar sources, *The Journal of the Acoustical Society of America* 104(5) (1998) 2845-2850.

[32] E. Fernandez-Grande, F. Jacobsen, and Q. Leclère, Direct formulation of the

supersonic acoustic intensity in space domain, *The Journal of the Acoustical Society of America* 131(1) (2012) 186-193.

[33] L.X. Zhao, S.C. Conlon, and F. Semperlotti, Broadband energy harvesting using acoustic black hole structural tailoring, *Smart Materials and Structures* 23(2014) 065021.

[34] P.A. Feurtado and S.C. Conlon, Wavenumber transform analysis for acoustic black hole design, *The Journal of the Acoustical Society of America* 140(1) (2016) 718-727.

[35] F. Fahy, and P. Gardonio, Sound and structural vibration: radiation, transmission and response, *Elsevier* 2009.

[36] ISO 3744: 2009, Acoustic-Determination of sound power levels of noise sources using sound pressure-engineering method in an essentially free field over a reflecting plane. *Brussels: International Organization for Standardization* 2009.